Numerical solution of frictional contact problems based on a mortar algorithm with an augmented Lagrangian technique

F. J. Cavalieri & A. Cardona

Multibody System Dynamics

ISSN 1384-5640

Multibody Syst Dyn
DOI 10.1007/s11044-015-9449-8

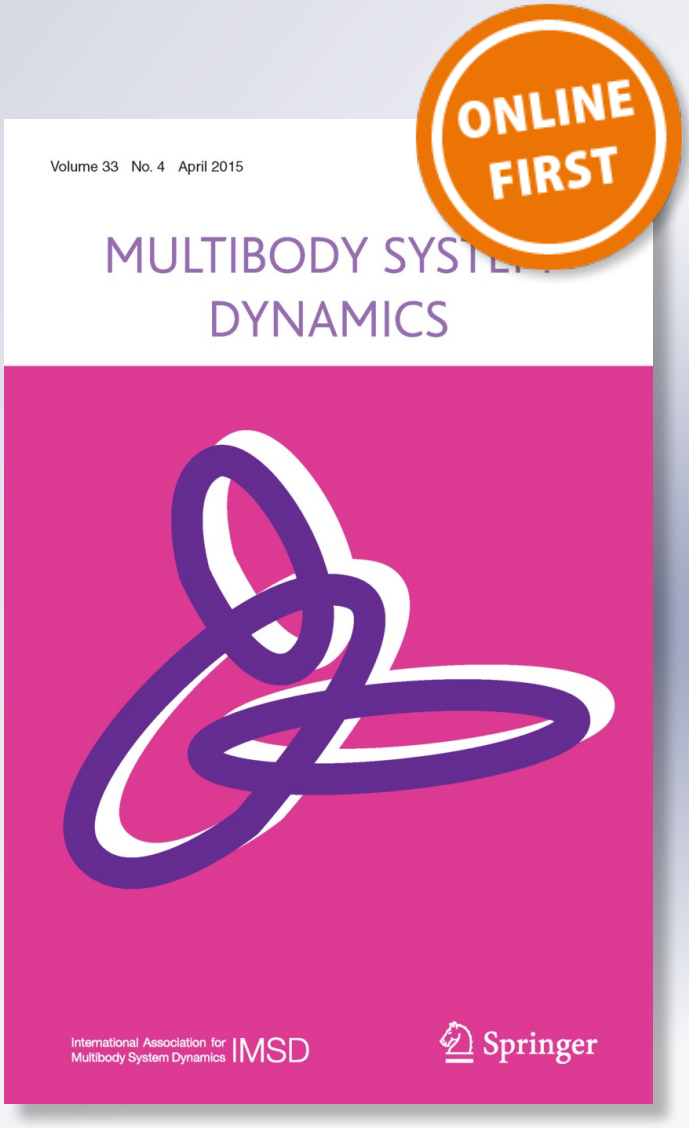

Springer

Multibody Syst Dyn
DOI 10.1007/s11044-015-9449-8

Numerical solution of frictional contact problems based on a mortar algorithm with an augmented Lagrangian technique

F.J. Cavalieri[1] · **A. Cardona**[1]

Received: 24 July 2014 / Accepted: 30 January 2015

Abstract This work presents a frictional contact formulation to solve three-dimensional contact problems with large finite displacements. The kinematic description of the contacting bodies is defined by using a mortar approach. The regularization of the variational frictional contact problem is solved with a mixed dual penalty approach based on an augmented Lagrangian technique. In this method, the numerical results do not depend on the definition of any user-defined penalty parameter affecting the normal or tangential component of forces. The robustness and performance of the proposed algorithm are studied and validated by solving a series of numerical examples with finite displacements and large slip.

Keywords Friction · Contact mechanics · Mortar method · Augmented Lagrangian

1 Introduction

Contact mechanics refers to the study of the stress and deformation of two bodies that touch each other [37]. Applications of contact mechanics in engineering problems are diverse, for example, the design of gears [22], studies of wear or tribology processes [8, 11, 36], applications in metal forming [19], and many others. The first study of contact mechanics dates from 1882 with the publication "On the contact of elastic solids" by Heinrich Hertz. The solutions of the Hertzian contact problems are restricted to elastic solids with simple boundary conditions, which limit their application to real world general problems. Currently, the Finite Element Method (FEM) is the most popular numerical technique for the analysis of complex problems that involve contact mechanics. Through the years, many researchers have proposed different approximations and algorithms to calculate, with robustness and accuracy, the stress and deformation of the contacting bodies. However, due to the nonlinearity

✉ A. Cardona
acardona@unl.edu.ar

[1] Centro de Investigación de Métodos Computacionales (CIMEC), Universidad Nacional del Litoral/CONICET, Predio CONICET-Santa Fe, Colectora Ruta Nac. 168/Paraje El Pozo, 3000 Santa Fe, Argentina

Published online: 27 March 2015

of the problem, there is not yet a completely robust contact algorithm suitable for a wide range of applications, and for this reason contact mechanics is still an active research area.

A widely widespread technique in the framework of the FEM for the description of the relative displacement between two contacting bodies is the node-to-segment approach where a node of one body (the *master* body) is associated with a segment (2D case) or a surface (3D case) of the other body (the *slave* body). An extensive list of references with different variants and practical applications of this method can be found in the books of Wriggers [68] and Laursen [43]. The main drawback of the node-to-segment approach is that it is unable to pass the contact patch test [49] and, therefore, displays jumps in the computed contact pressure when the slave nodes slide between non-smooth adjacent segments or surfaces, producing ill-conditioned matrices and a poor convergence rate [56]. The double pass node-to-segment approach satisfies the contact patch test, but it can "lock" due to the over-restriction introduced in the formulation [56].

Another method proposed to simulate contact mechanics problems is the so-called segment-to-segment approach where the segment of one body (the *master* segment) is associated with a segment of the another body (a *slave* segment). Most of the segment-to-segment methods use some kind of intermediate surface or projection surface. The surface-surface mortar strategy was originally proposed as a domain decomposition method and was used to solve finite element problems with non-conforming discretizations. An important characteristic of the mortar method is that it is one pass only, and verifies the contact patch tests. Therefore, a double pass proposal would be completely unnecessary. Specifically, the first work that used the mortar method was published by Bernardi et al. [4], where the authors demonstrated the stability properties related with the Babuska–Brezzi conditions [6]. The first proposals of the mortar method used in engineering applications were introduced in the context of infinitesimal displacements [44]. Then, many authors extended the mortar approximation to problems with large finite displacements, large sliding or time dependent problems [12, 13, 17, 28–30, 33–35, 50, 51, 53, 56]. Even though the references [38, 48, 60, 61] are not usually considered as mortar methods, they incorporate all the characteristics to be classified as mortar [63]. Recently, Temizer [63], De Lorenzis et al. [15] and Kim and Youn [40] applied the mortar method in the context of isogeometric analysis.

The treatment of the contact restrictions can be addressed by different strategies: by using a penalty approach, Lagrange multipliers or augmented Lagrangian techniques within many others. For example, in the works of Puso and Laursen [56] and Yang et al. [69], a mortar formulation with a penalty method is presented. Puso [53] proposed a mortar method based on an augmented Lagrangian combined with a double loop Uzawa-type algorithm. Later, Popp et al. [50] proposed a mortar algorithm where a dual Lagrange multipliers is used, and recently, Cavalieri and Cardona [10] proposed a frictionless mortar contact algorithm combined with an augmented Lagrangian method. Each one of these proposals has advantages and disadvantages as described, e.g., in [10, 52].

The complexity of the numerical solutions in contact mechanics is increased when friction is taken into account. The first mathematical formulation of frictional contact problems was proposed more than 200 years ago by Coulomb, and then followed by Hertz. Despite the great efforts made to explain the friction process, until today there is no total consensus on a global theory that adequately describes this complex phenomenon. In fact, friction is strongly influenced by the interaction of different tribological properties such as the lubrication conditions, the plastic deformations and the geometric changes of the contact surfaces, which increase the difficulty of the analysis.

The global convergence rate of contact algorithms is degraded as a consequence of the consideration of friction [16]. In most cases, friction is modeled by using the Coulomb law.

This is an approximated law, which considers only one parameter in the formulation: the friction coefficient. Although this law is very simple, it allows describing with an acceptable approximation a wide range of real world applications. In the Coulomb law, the normal force is independent of friction, and so, a non-symmetric system of equations is obtained [45].

Several works proposed friction contact algorithms combined with mortar methods. For instance, Puso and Laursen [55] proposed a mortar method with a penalty regularization within an augmented Lagrangian scheme [39]. The works of Yang et al. [69] and Fischer and Wriggers [18] presented a penalty method for the regularization of the variational problem and a mortar approach to describe the contact kinematics. Heintz and Hansbo [32] proposed a stabilized Lagrange multiplier method based on a global polynomial multiplier for the finite element solution of nonlinear elastic contact problems with non-matching grids in 2D. In the works of Oliver et al. [47] and Hartmann et al. [27], a computational contact strategy utilizes a stabilized Lagrange multiplier formulation for the enforcement of the contact constraints in 2D. Although this method is not a mortar approach, it incorporates a fictitious intermediate region that connects the potential contact surfaces. In the work of Tur et al. [66], the correct contact conditions for every slave node in a gap, stick or slip statuses are evaluated in an internal loop, whereas an external loop is used to solve the nonlinear equation using Newton's method. This method has a disadvantage related with the higher computational cost due to the two nested loops and, a special modification of the classical Newton solver is required. More recently, Gitterle et al. [25] proposed a two-dimensional finite deformation frictional contact formulation based on a mortar formulation. In this case, the enforcement of contact constraints is reached with dual Lagrange multipliers. By using the so-called dual mortar method [67], it is possible to eliminate the Lagrange multipliers from the set of linear equations by static condensation. However, the dual method may lack robustness, e.g., when contact surfaces have large curvatures or when one contacting body slips over an edge of the other contacting body. A more robust version of this method has been presented recently by Popp et al. [52].

In the work of De Lorenzis et al. [14], they focus on the application of NURBS-based isogeometric analysis to Coulomb frictional contact problems between deformable bodies in the context of large deformations and using the classical return mapping algorithm. A three-dimensional mortar-based frictional contact treatment in NURBS isogeometric analysis under the finite deformation regime is presented by Temizer et al. [64, 65]. In both works, a penalty approach supplemented by Uzawa augmentations is implemented for the regularization of the contact constraints.

In this work, an augmented Lagrangian technique combined with a mortar approach is proposed to solve three dimensional contact friction problems. The method is an extension of the frictionless mortar method presented by Cavalieri and Cardona [10]. Unlike the works mentioned above, the exact enforcement of the contact and friction constraints is obtained by using the augmented Lagrangian method proposed by Alart and Curnier [1]. In agreement with the comments of De Lorenzis et al. [15], this method has remarkable robustness, yields quadratic convergence, is relatively easy to incorporate into a nonlinear finite element code, and contrary to the penalty method, no artificial parameter is introduced for the regularization of the problem. The system of equations, including the Lagrange multipliers is linearized and solved by a monolithic Newton–Raphson method. Thus, it is not necessary to implement a three-nested-loops scheme as in the Uzawa type method, avoiding any modification of a pre-existing Newton solver.

An example with small deformations is presented to validate the proposed algorithm with a classical frictional benchmark. Then, three examples in the framework of 3D finite displacements are presented to demonstrate the applicability and robustness of the proposed

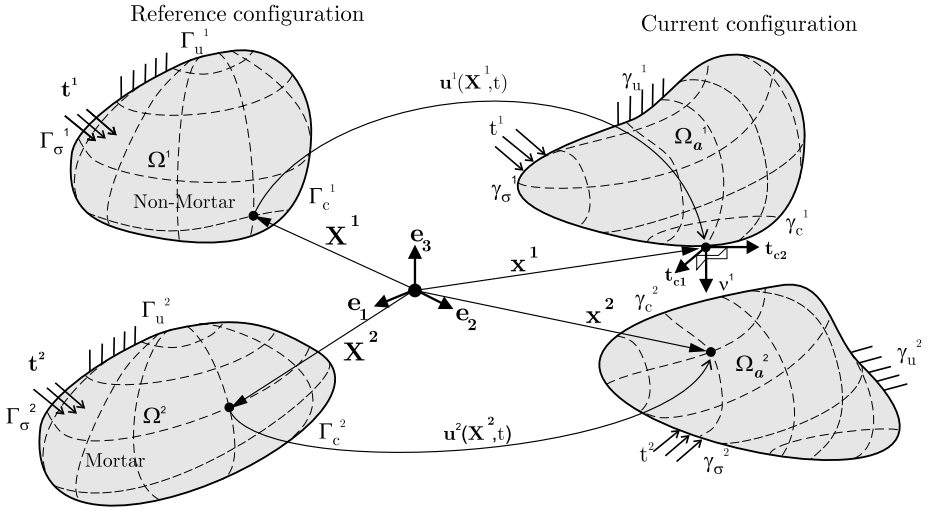

Fig. 1 Two-body contact problem in the framework of large displacements

algorithm. In all cases, the normal and tangential stress solutions are smooth, even with non-conforming meshes, demonstrating the validity of the formulation.

2 Problem description

Figure 1 depicts the contact problem for finite deformations. The contacting bodies $\mathcal{B}^\alpha$, $\alpha = 1, 2$, occupy the open set $\Omega^\alpha \subset \mathbb{R}^3$ in the reference configuration and $\Omega_a^\alpha \subset \mathbb{R}^3$ in the current configuration. The external surface $\partial\Omega^\alpha$ in the reference configuration is divided into three disjoints parts: Γ_u^α where the body is fixed, Γ_σ^α where the surface traction vector is acting, and Γ_c^α which represents the contact boundary. The same boundaries in the current configuration are denoted as γ_u^α, γ_σ^α and γ_c^α, respectively.

In the reference configuration, the material points for each solid are denoted by the position vector $\boldsymbol{X}^\alpha \in \Omega^\alpha$, while in the current configuration they are given by the vector $\boldsymbol{x}^\alpha \in \Omega_a^\alpha$. Then, the movement of both bodies is described by the displacement field $\boldsymbol{u}^\alpha$ which is related to the reference and current positions by $\boldsymbol{x}^\alpha = \boldsymbol{X}^\alpha + \boldsymbol{u}^\alpha$. The total potential energy for the contacting bodies $\mathcal{B}^\alpha$ is given by

$$\Pi = \Pi^{\mathrm{c}} + \Pi^{\mathrm{int,ext}}, \tag{1}$$

where Π^{c} is the contact potential energy and $\Pi^{\mathrm{int,ext}}$ represents the potential energy of the external and internal loads. In the case of a hyperelastic material, $\Pi^{\mathrm{int,ext}}$ yields

$$\Pi^{\mathrm{int,ext}} = \sum_{\alpha=1}^{2}\left[\int_{\Omega^\alpha}\left(W^\alpha\left(\boldsymbol{C}^\alpha\right) - \boldsymbol{b}^\alpha \cdot \boldsymbol{u}^\alpha\right) d\Omega - \int_{\Gamma_N^\alpha} \hat{\boldsymbol{t}}^\alpha \cdot \boldsymbol{u}^\alpha \, d\Gamma\right]. \tag{2}$$

Here, $\boldsymbol{b}^\alpha$ is the body force vector in Ω^α, $\hat{\boldsymbol{t}}^\alpha$ is the prescribed traction vector, W^α is the strain energy density function for a hyperelastic material and $\boldsymbol{C}^\alpha = (\boldsymbol{F}^{\alpha\,T}\boldsymbol{F}^\alpha)$ is the right Cauchy–Green deformation tensor with $\boldsymbol{F}^\alpha$ representing the deformation gradient.

The simplest representation of W^α is the Saint Venant–Kirchhoff model, from which the second Piola–Kirchhoff stress tensor $\boldsymbol{S}^\alpha$ and the fourth-order constitutive tensor $\boldsymbol{D}^\alpha$ are derived by the following relations:

$$\boldsymbol{S}^\alpha = \frac{\partial W^\alpha}{\partial \boldsymbol{E}^\alpha}, \qquad \boldsymbol{D}^\alpha = \frac{\partial^2 W^\alpha}{\partial \boldsymbol{E}^\alpha \partial \boldsymbol{E}^\alpha}, \tag{3}$$

where $\boldsymbol{E}^\alpha$ is the Green–Lagrange strain tensor defined as

$$\boldsymbol{E}^\alpha = \frac{1}{2}\left(\boldsymbol{F}^{\alpha\,T}\boldsymbol{F}^\alpha - \boldsymbol{I}\right). \tag{4}$$

This work puts emphasis on the solution of the contact equations; then, no details about modeling of solid deformation will be presented. The potential energy due exclusively to contact is given by

$$\Pi^{\mathrm{c}} = -\sum_{\alpha=1}^{2} \int_{\gamma_c^\alpha} \bar{\boldsymbol{t}}_c^{\,\alpha} \cdot \boldsymbol{x}^\alpha \, d\gamma, \tag{5}$$

where $\bar{\boldsymbol{t}}_c^{\,\alpha}$ is the Cauchy stress vector of the body $\mathcal{B}^\alpha$ in the current configuration. Assuming linear momentum balance at the contact surface, $\bar{\boldsymbol{t}}_c^{\,1}\, d\gamma^1 = -\bar{\boldsymbol{t}}_c^{\,2}\, d\gamma^2$, the contact potential energy can be simplified as

$$\Pi^{\mathrm{c}} = -\int_{\gamma_c^1} \bar{\boldsymbol{t}}_c^{\,1} \cdot \left(\boldsymbol{x}^1 - \boldsymbol{x}^2\right) d\gamma. \tag{6}$$

Instead of using the Cauchy stress vector $\bar{\boldsymbol{t}}_c^{\,1}$, a vector field $\boldsymbol{\lambda} = -\bar{\boldsymbol{t}}_c^{\,1}$ is introduced. This field can be seen as the Lagrange multiplier field that enforces the verification of the constraint $\boldsymbol{x}^1 = \boldsymbol{x}^2$ at the interface between bodies in contact. The physical interpretation of this Lagrange multiplier is clear from the equations above: it is the negative surface traction vector defined on the contact surface γ_c^1 which enforces the contact conditions between bodies, and represents the force produced by body 2 (the mortar) over body 1 (the non mortar body). Thus, the contact potential energy in Eq. (6) is re-written as

$$\Pi^{\mathrm{c}} = \int_{\gamma_c^1} \boldsymbol{\lambda} \cdot \left(\boldsymbol{x}^1 - \boldsymbol{x}^2\right) d\gamma. \tag{7}$$

We remark that in this work we are analyzing the static problem. When dealing with a dynamic problem, some other terms are usually added to account for the local dynamics at the contact zone, and to damp-out local oscillations. Several proposals exist, such as those of Flores and Ambrósio [20], Bowling et al. [5] or Förg et al. [21], among many others. This kind of modifications can also be incorporated in this formulation.

The finite element method is used to discretize the bodies domains. The position fields $\boldsymbol{x}^\alpha : \gamma_c^\alpha \to \mathbb{R}^3$, which describe the contact surfaces of each body and the Lagrange multipliers vector field $\boldsymbol{\lambda} : \gamma_c^1 \to \mathbb{R}^3$, can be parameterized as follows [53]:

$$\boldsymbol{x}^\alpha = \sum_{A=1}^{n^\alpha} N_A^\alpha\left(\boldsymbol{\xi}^\alpha\right)\boldsymbol{x}_A^\alpha, \quad \alpha = 1, 2, \qquad \boldsymbol{\lambda} = \sum_{A=1}^{n^1} N_A^1\left(\boldsymbol{\xi}^1\right)\boldsymbol{\lambda}_A, \tag{8}$$

where $\boldsymbol{x}_A^\alpha$ are the nodal coordinates, $\boldsymbol{\xi}^\alpha$ are the local coordinates, n^α is the number of nodes in γ_c^α, and $N_A^\alpha : \gamma_c^\alpha \to \mathbb{R}$ are the classical shape functions of the FEM discretization. As

usually named in the literature, γ_c^1 and γ_c^2 are the non-mortar and mortar surfaces in the current configuration, respectively. The nodal discrete Lagrange multipliers $\boldsymbol{\lambda}_A$ approximate the Lagrange multipliers field with the same shape functions used to approximate the geometry and the displacements. By using Eqs. $(8)_{1,2}$ and Eq. (7), the contact potential energy in the framework of the FEM is expressed as

$$\Pi^{\mathrm{c}} = \sum_{A=1}^{n^1} \boldsymbol{\lambda}_A \cdot \left(\sum_{B=1}^{n^1} \int_{\gamma_c^1} N_A^1(\boldsymbol{\xi}^1) N_B^1(\boldsymbol{\xi}^1)\, d\gamma\, \boldsymbol{x}_B^1 - \sum_{C=1}^{n^2} \int_{\gamma_c^1} N_A^1(\boldsymbol{\xi}^1) N_C^2(\boldsymbol{\xi}^2)\, d\gamma\, \boldsymbol{x}_C^2 \right) \tag{9}$$

where the term in parentheses can be interpreted as an average measure of the gap and transversal relative displacement corresponding to the node A. Therefore,

$$\Pi^{\mathrm{c}} = \sum_{A=1}^{n^1} \boldsymbol{\lambda}_A \cdot \boldsymbol{g}_A, \tag{10}$$

with

$$\boldsymbol{g}_A = \sum_{B=1}^{n^1} \int_{\gamma_c^1} N_A^1(\boldsymbol{\xi}^1) N_B^1(\boldsymbol{\xi}^1)\, d\gamma\, \boldsymbol{x}_B^1 - \sum_{C=1}^{n^2} \int_{\gamma_c^1} N_A^1(\boldsymbol{\xi}^1) N_C^2(\boldsymbol{\xi}^2)\, d\gamma\, \boldsymbol{x}_C^2, \tag{11}$$

namely the generalized gap vector at node A.

3 Friction contact problem

When friction is considered, the generalized gap vector $\boldsymbol{g}_A$ and the Lagrange multiplier $\boldsymbol{\lambda}_A$ can be split into the normal components g_{NA} and λ_{NA}, and the tangential components $\boldsymbol{g}_{TA}$ and $\boldsymbol{\lambda}_{TA}$. The splitting is carried out using the average outward normal vector $\boldsymbol{v}_A$ to the surface γ_c^1 at node A. The equations are defined for quasi-static problems where the time period of analysis $[0, T]$ is subdivided into time intervals $[t_n, t_{n+1}]$ with the corresponding time step $\Delta t = t_{n+1} - t_n$. In this way, the contact potential energy can be divided into normal and tangential components, yielding

$$\begin{aligned}
\Pi^{\mathrm{c}} = \sum_{A=1}^{n^1} \Bigg[& \lambda_{NA}(t_{n+1}) \\
& \times \underbrace{\boldsymbol{v}_A(t_n) \cdot \left(\sum_{B=1}^{n^1} n_{AB}^1(t_{n+1}) \boldsymbol{x}_B^1(t_{n+1}) - \sum_{C=1}^{n^2} n_{AC}^2(t_{n+1}) \boldsymbol{x}_C^2(t_{n+1}) \right)}_{g_{NA}} \\
& + \boldsymbol{\lambda}_{TA}(t_{n+1}) \\
& \cdot \underbrace{\left[\boldsymbol{I} - \boldsymbol{v}_A(t_n) \otimes \boldsymbol{v}_A(t_n) \right] \left(\sum_{B=1}^{n^1} n_{AB}^1(t_{n+1})\, \boldsymbol{x}_B^1(t_n) - \sum_{C=1}^{n^2} n_{AC}^2(t_{n+1})\, \boldsymbol{x}_C^2(t_n) \right)}_{\boldsymbol{g}_{TA}} \Bigg]
\end{aligned} \tag{12}$$

where n^1_{AB} and n^2_{AB} are the weight factors defined as

$$n^1_{AB} = \int_{\gamma_c^1} N^1_A(\boldsymbol{\xi}^1) N^1_B(\boldsymbol{\xi}^1)\, d\gamma, \qquad n^2_{AC} = \int_{\gamma_c^1} N^1_A(\boldsymbol{\xi}^1) N^2_C(\boldsymbol{\xi}^2)\, d\gamma. \tag{13}$$

Note that in the term corresponding to the normal component of Eq. (12), the weight factors n^α_{AB} and the positions $\boldsymbol{x}^\alpha_A$ are evaluated at the current time step t_{n+1}, while in the tangential component term, the positions are evaluated at the previous time step t_n. This way of defining the tangential component allows representing the incremental tangential movement and ensuring objectivity properties in the formulation, as demonstrated by Puso and Laursen [55]. Note also that to simplify the formulation, the outward unit normal vector $\boldsymbol{v}_A$ is evaluated explicitly at the previous time step t_n. The contact potential energy term is therefore finally written as

$$\Pi^{\mathrm{c}} = \sum_{A=1}^{n^1} \lambda_{NA}(t_{n+1}) g_{NA}(t_{n+1}) + \boldsymbol{\lambda}_{TA}(t_{n+1}) \cdot \boldsymbol{g}_{TA}(t_{n+1}). \tag{14}$$

In what follows, the time variable t will be omitted from the equations to simplify the notation.

3.1 General solution of the friction contact problem

The general solution to the unilateral friction contact problem by a mortar formulation is then given by

$$\begin{aligned} &\boldsymbol{U} = \operatorname{arginf}\left(\Pi^{\mathrm{int,ext}}(\boldsymbol{U}) + \Pi^{c}(\boldsymbol{U})\right), \\ &\quad \text{s.t.} \quad g_{NA} \geq 0, \quad \lambda_{NA} \leq 0, \quad \lambda_{NA} g_{NA} = 0; \\ &\qquad \|\boldsymbol{\lambda}_{TA}\| \leq -\mu\lambda_{NA}, \quad \boldsymbol{g}_{TA} = \|\boldsymbol{g}_{TA}\| \frac{\boldsymbol{\lambda}_{TA}}{\|\boldsymbol{\lambda}_{TA}\|}, \quad \|\boldsymbol{g}_{TA}\|\left(\|\boldsymbol{\lambda}_{TA}\| + \mu\lambda_{NA}\right) = 0; \\ &\qquad A = 1, \ldots, n^1, \end{aligned} \tag{15}$$

where $\boldsymbol{U}$ is the global displacements vector. The first set of restrictions in Eq. (15) represents the Karush–Kuhn–Tucker conditions (KKT) for the unilateral frictionless contact problem. The first condition indicates the impenetrability restriction, the second one is the non-traction condition (only compression is allowed) and the third one is the complementarity equation. The second set of restrictions represents the KKT conditions for friction. The first inequality establishes the maximum value of the tangential contact pressure, $\mu\lambda_{NA}$, where μ is the friction coefficient. The second equation imposes the collinearity between the tangential displacement and the tangential contact stress (an associative slip rule is assumed). The third one is the complementary equation which indicates that $\boldsymbol{g}_{TA}$ and $\|\boldsymbol{\lambda}_{TA}\| + \mu\lambda_{NA}$ cannot be simultaneously zero. Hence, when $\|\boldsymbol{\lambda}_{TA}\| < -\mu\lambda_{NA}$ and $\boldsymbol{g}_{TA} = 0$ the contact status is in stick, and when $\boldsymbol{g}_{TA} \neq 0$, the tangential stresses are equal to $\|\boldsymbol{\lambda}_{TA}\| = -\mu\lambda_{NA}$ and the body slips. The consideration of friction presents an additional complexity with respect to the frictionless problem, which is related to the successive changes of status from stick to slip or vice versa.

A popular method to solve the friction contact problem is by a penalty approach together with a *return mapping* algorithm [23, 59]. Here, in the stick status, the tangential force

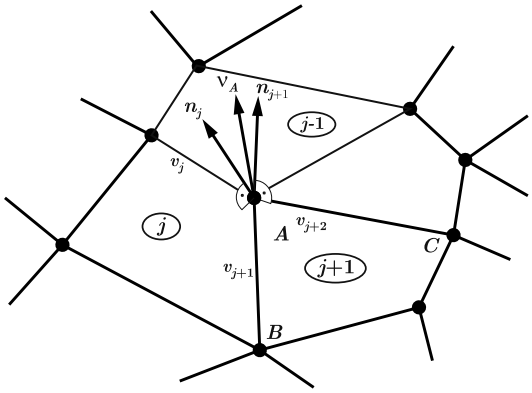

Fig. 2 Outward unit normal vector calculation

depends linearly on a small slip quantity via an artificial penalty parameter. The first disadvantage of this method is that the user has to find a correct value of the penalty parameter by trial and error, which implies multiple runs for tuning. Furthermore, some numerical difficulties appear in the stick condition due to the high value of penalty needed to properly simulate this state, producing an ill-conditioned stiffness matrix. In addition, in the slip state the tangent stiffness matrix is non-symmetric because the tangential force is independent of the normal component of displacement. These drawbacks are overcome by using the augmented Lagrangian method as proposed by Simo and Laursen [58] and Laursen [42], where the friction force arises from a Lagrange multiplier evaluated in the previous iteration, which produces a symmetric stiffness matrix. This approach is combined with an Uzawa-type algorithm. However, the computational cost is relatively high because of the need of two nested loops in the Uzawa algorithm.

In this work, the friction contact problem presented in Eq. (15) is solved as a minimization problem with inequality constraints by using an augmented Lagrangian formulation, where the values which make the functional stationary are solved in only one loop.

3.2 Normal vector

A unique normal vector $\boldsymbol{v}_A$ at node A is calculated by averaging the normal vectors to the non-mortar elements attached to this node (see Fig. 2):

$$\boldsymbol{v}_A = \frac{\sum_j^{n_1} \boldsymbol{n}_j}{\|\boldsymbol{n}_j\|}, \tag{16}$$

where

$$\boldsymbol{n}_j = \frac{\boldsymbol{v}_j \times \boldsymbol{v}_{j+1}}{\|\boldsymbol{v}_j \times \boldsymbol{v}_{j+1}\|} \tag{17}$$

is the normal vector to the non-mortar element j at node A, and the vectors $\boldsymbol{v}_j$ and $\boldsymbol{v}_{j+1}$ are calculated from the differences of the nodal coordinates,

$$\begin{aligned} \boldsymbol{v}_{j+1} &= \boldsymbol{x}_C^1 - \boldsymbol{x}_A^2, \\ \boldsymbol{v}_j &= \boldsymbol{x}_B^1 - \boldsymbol{x}_A^2. \end{aligned} \tag{18}$$

In the frictionless case, we worked with contact forces defined in terms of a different normal vector at each non-mortar facet evaluated at node A. In this way, a scalar value

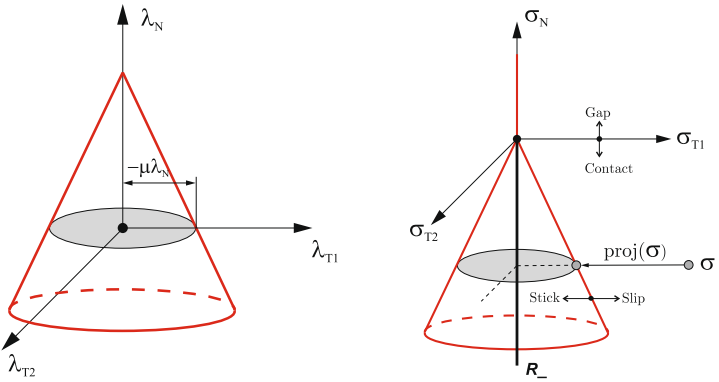

(a) Coulomb's isotropic friction cone.

(b) Extension of the augmented Coulomb's isotropic friction cone.

Fig. 3 Three dimensional representation of the Coulomb's friction cone

of the contact force was computed, as an average of the contact forces coming from the contributions of each facet [10].

However, in the frictional case, it is of utmost importance to define a single normal vector at the node. Otherwise, the tangent components of the contact stress vector would not be computed correctly, their directions would change with the iterations, and consequently, the contact forces of the element (see Eq. (12)) would switch iteratively between the stick or slip status, severely affecting the convergence of the Newton iterations.

In order to simplify the formulation, the outward unit normal vector $\boldsymbol{\nu}_A$ is evaluated explicitly at the previous time step t_n; in this way, it does not have any contribution to the Hessian matrix, simplifying its computation.

4 Augmented Lagrangian formulation

The inequality constraints of the first set of restrictions in Eq. (15) that corresponds to the unilateral contact problem can be equivalently written as the sub-differential inclusion

$$\lambda_{NA} \in \partial \Psi_{R^+}(g_{NA}), \tag{19}$$

where $\Psi_{\boldsymbol{R}_+}$ is the indicator function of the real half line $\boldsymbol{R}_+$ and $\partial \Psi_{\boldsymbol{R}_+}$ is the sub-differential of $\Psi_{\boldsymbol{R}_+}$. Equation (19) expresses the unilateral contact conditions, with a contact pressure field derived from a non-smooth potential $\Psi_{\boldsymbol{R}_+}(g_{NA})$ [1, 31]. The last set of constraints of Eq. (15) that refer to the contact friction problem has the following sub-differential inclusion:

$$\boldsymbol{\lambda}_{TA} \in \partial \Psi_C^*(\boldsymbol{g}_{TA}), \tag{20}$$

where Ψ_C^* is the conjugate function of Ψ_C and $\partial \Psi_C^*$ is its sub-differential [1]. In three-dimensional problems, the Coulomb's isotropic friction law is represented by a cone, as shown in Fig. 3(a). A section of the Coulomb's cone of radius $-\mu\lambda_{NA}$ is defined by

$$C(\lambda_{NA}) = \left\{ \boldsymbol{\lambda}_{TA} / \|\boldsymbol{\lambda}_{TA}\| \leq -\mu\lambda_{NA} \right\}. \tag{21}$$

Equation (15) can be regularized and solved using a mixed dual formulation based on an augmented Lagrangian method, as proposed in Alart and Curnier [1, 21]. The potential energy of contact (14) is replaced by an augmented Lagrangian function, which is defined by

$$\mathcal{L}^c(\boldsymbol{U},\boldsymbol{\lambda}) = \sum_{A=1}^{n^1}\Big(k g_{NA}\lambda_{NA} + \frac{r}{2}\big\|g_{NA}(\boldsymbol{U})\big\|^2 - \frac{1}{2r}\mathrm{dist}^2\big[k\lambda_{NA} + r g_{NA}(\boldsymbol{U}), R^-\big] + k\boldsymbol{g}_{TA}\boldsymbol{\lambda}_{TA} + \frac{r}{2}\big\|\boldsymbol{g}_{TA}(\boldsymbol{U})\big\|^2 - \frac{1}{2r}\mathrm{dist}^2\big[k\boldsymbol{\lambda}_{TA} + r\boldsymbol{g}_{TA}(\boldsymbol{U}), C^{\mathrm{augm}}\big]\Big) \tag{22}$$

where r is a positive penalty parameter, k is a positive scale factor, $\mathrm{dist}(x, C)$ is the distance between x and C. The term $k\boldsymbol{\lambda}_A + r\boldsymbol{g}_A$ is the so-called *augmented Lagrange multiplier*

$$\boldsymbol{\sigma}_A = k\boldsymbol{\lambda}_A + r\boldsymbol{g}_A = \sigma_{NA}\boldsymbol{v}_A + \boldsymbol{\sigma}_{TA}, \tag{23}$$

with normal part σ_{NA} and tangential part $\boldsymbol{\sigma}_{TA}$:

$$\begin{aligned} \sigma_{NA} &= k\lambda_{NA} + r g_{NA}, \\ \boldsymbol{\sigma}_{TA} &= k\boldsymbol{\lambda}_{TA} + r\boldsymbol{g}_{TA}. \end{aligned} \tag{24}$$

The extended cone C^{augm} is the convex set defined by extension of the friction cone $C(k\lambda_{NA} + r g_{NA}) \equiv C(\sigma_{NA})$ to the half-line $R^+(\sigma_{NA})$, i.e., the set of positive values of the normal augmented Lagrange multiplier, see Fig. 3(b).

The solution does not depend on the value of parameters r, k. Nevertheless, the convergence rate does depend on their value. In numerical computations, default values of r and k are selected in terms of a mean value of the Young modulus of the bodies in contact and of a mean value of mesh size as follows:

$$r = k \approx 10\frac{E_{\mathrm{mean}}}{h_{\mathrm{mean}}}. \tag{25}$$

Numerical tests showed that this choice gives a better condition number of the iteration matrix than other choices [10]. Eventually, different sets of values of r, k can be used for the normal and for the tangential parts.

5 Contact element definition

A *contact element* is defined for each pair of facets, one on the non-mortar and the other on the mortar surface. If $N1$ is the number of facets on the surface Γ_c^1, and $N2$ is the number of facets on the surface Γ_c^2, a total of $N1 \times N2$ contact elements are built. Note, however, that only a few of them are active at a given time (i.e., only those elements whose facets are seeing each other). At each contact element, the restrictions to the element facets of the integrals needed for the computation of the weight factors n_{AB}^1, n_{AB}^2 are evaluated. The weight factors are then obtained by assembling the contributions of all elements [10, 53].

The generalized coordinates of the contact element are

$$\boldsymbol{\Phi}^e = \big[\boldsymbol{x}_1^{1T}\ \boldsymbol{x}_2^{1T}\ \cdots\ \boldsymbol{x}_{m^1}^{1\ T}\ \boldsymbol{x}_1^{2T}\ \boldsymbol{x}_2^{2T}\ \cdots\ \boldsymbol{x}_{m^2}^{2\ T}\ \boldsymbol{\lambda}_1^T\ \boldsymbol{\lambda}_2^T\ \cdots\ \boldsymbol{\lambda}_{m^1}^T\big]^T, \tag{26}$$

where m^1 and m^2 are the number of nodes of the non-mortar facet and the mortar facet, respectively, $\boldsymbol{x}_I^1$ are the nodal coordinates of the non-mortar facet, $\boldsymbol{x}_I^2$ are the nodal coordinates of the mortar facet, and $\boldsymbol{\lambda}_I$ are the contact nodal forces. The total number of degrees of freedom of the contact element is $6m^1 + 3m^2$.

6 Internal force vector

The internal force vector for a contact element is obtained by taking variations in $\mathcal{L}^c$, see Eq. (22), thus,

$$\delta\mathcal{L}^c = \sum_{A=1}^{n^1} \begin{bmatrix} \delta\boldsymbol{x}_B^1 \\ \delta\boldsymbol{x}_C^2 \\ \delta\boldsymbol{\lambda}_A \end{bmatrix} \cdot \begin{bmatrix} n_{AB}^1[\text{proj}_{R^-}(\sigma_{NA})\boldsymbol{v}_A + \text{proj}_{C^{\text{augm}}}(\boldsymbol{\sigma}_{TA})] \\ -n_{AC}^2[\text{proj}_{R^-}(\sigma_{NA})\boldsymbol{v}_A + \text{proj}_{C^{\text{augm}}}(\boldsymbol{\sigma}_{TA})] \\ -\frac{k}{r}[k\lambda_{NA} - \text{proj}_{R^-}(\sigma_{NA})]\boldsymbol{v}_A - \frac{k}{r}[k\boldsymbol{\lambda}_{TA} - \text{proj}_{C^{\text{augm}}}(\boldsymbol{\sigma}_{TA})] \end{bmatrix}, \tag{27}$$

where $\text{proj}_{R^-}(\sigma_{NA})$ is the projection of σ_{NA} on R^-:

$$\text{proj}_{R^-}(\sigma_{NA}) = \begin{cases} \sigma_{NA} & \text{if } \sigma_{NA} < 0, \\ 0 & \text{if } \sigma_{NA} \geq 0. \end{cases} \tag{28}$$

The projection operator $\text{proj}_{C^{\text{augm}}}(\boldsymbol{\sigma}_{TA})$ is defined as

$$\text{proj}_{C^{\text{augm}}}(\boldsymbol{\sigma}_{TA}) = \begin{cases} \boldsymbol{\sigma}_{TA} & \text{if } \|\boldsymbol{\sigma}_{TA}\| \leq \rho, \\ \rho\boldsymbol{t}_A & \text{if } \|\boldsymbol{\sigma}_{TA}\| > \rho, \end{cases} \tag{29}$$

where $\rho = -\mu\sigma_{NA}$ corresponds to the radius of the disk in the friction Coulomb cone and $\boldsymbol{t}_A$ is the tangential unit vector in the slip direction at node A:

$$\boldsymbol{t}_A = \frac{\boldsymbol{\sigma}_{TA}}{\|\boldsymbol{\sigma}_{TA}\|}. \tag{30}$$

The contact status (*gap*, *stick* or *slip*) is determined in terms of the value of the normal component of the augmented Lagrange multiplier σ_{NA}. The condition $\sigma_{NA} \geq 0$ is associated to the *gap* condition, in this case, $\text{proj}_{R^-}(\sigma_{NA}) = 0$ and $\text{proj}_{C^{\text{augm}}}(\boldsymbol{\sigma}_{TA}) = \boldsymbol{0}$. For these reasons, from Eq. (27), the contribution of node A to the internal contact force vector yields

$$\boldsymbol{F}^{cA} = \begin{bmatrix} \boldsymbol{0} \\ \boldsymbol{0} \\ -\frac{k^2}{r}\boldsymbol{\lambda}_A \end{bmatrix}. \tag{31}$$

The *stick* condition is obtained when $\|\boldsymbol{\sigma}_{TA}\| < -\mu\sigma_{NA}$. In this case, $\text{proj}_{R^-}(\sigma_{NA}) = \sigma_{NA}$ and $\text{proj}_{C^{\text{augm}}}(\boldsymbol{\sigma}_{TA}) = \boldsymbol{\sigma}_{TA}$. Therefore, from Eq. (27), the contribution of node A to the internal contact force vector yields

$$\boldsymbol{F}^{cA} = \begin{bmatrix} n_{AB}^1\boldsymbol{\sigma}_A \\ -n_{AC}^2\boldsymbol{\sigma}_A \\ k\boldsymbol{g}_A \end{bmatrix}. \tag{32}$$

Finally, the slip condition is produced for $\|\boldsymbol{\sigma}_{TA}\| \geq -\mu\sigma_{NA}$. In this case, $\text{proj}_{R^-}(\sigma_{NA}) = \sigma_{NA}$ and $\text{proj}_{C^{\text{augm}}}(\boldsymbol{\sigma}_{TA}) = -\mu\sigma_{NA}\boldsymbol{t}_A$. Thus, from Eq. (27), the contribution of node A to the

internal contact force vector yields

$$\boldsymbol{F}^{cA} = \begin{bmatrix} n^1_{AB}(\boldsymbol{v}_A - \mu \boldsymbol{t}_A \sigma_{NA}) \\ -n^2_{AC}(\boldsymbol{v}_A - \mu \boldsymbol{t}_A \sigma_{NA}) \\ k \boldsymbol{v}_A g_{NA} - \frac{k}{r}(\boldsymbol{\lambda}_{TA} + \mu \sigma_{NA} \boldsymbol{t}_A) \end{bmatrix}. \tag{33}$$

7 Hessian matrix

The linearization of the contact vector gives the contact Hessian matrix. The contributions to the Hessian matrix are, for the different contact conditions, as follows:

– *Gap* status $\sigma_{NA} \geq 0$,

$$\Delta \boldsymbol{F}^{cA} = \begin{bmatrix} \boldsymbol{0} \\ \boldsymbol{0} \\ -\frac{k^2}{r} \Delta \boldsymbol{\lambda}_A \end{bmatrix}. \tag{34}$$

– *Stick* status $\|\boldsymbol{\sigma}_{TA}\| < -\mu \sigma_{NA}$,

$$\Delta \boldsymbol{F}^{cA} = \begin{bmatrix} \Delta n^1_{AB} \boldsymbol{\sigma}_A + n^1_{AB} \Delta \boldsymbol{\sigma}_A \\ -\Delta n^2_{AC} \boldsymbol{\sigma}_A - n^2_{AC} \Delta \boldsymbol{\sigma}_A \\ \Delta \boldsymbol{g}_A \end{bmatrix}. \tag{35}$$

– *Slip* status $\|\boldsymbol{\sigma}_{TA}\| \geq -\mu \sigma_{NA}$,

$$\Delta \boldsymbol{F}^{cA} = \begin{bmatrix} \Delta n^1_{AB} \, (\boldsymbol{v}_A - \mu \boldsymbol{t}_A \sigma_{NA}) + n^1_{AB} \, \Delta (\boldsymbol{v}_A - \mu \boldsymbol{t}_A \sigma_{NA}) \\ -\Delta n^2_{AC} \, (\boldsymbol{v}_A - \mu \boldsymbol{t}_A \sigma_{NA}) - n^2_{AC} \, \Delta (\boldsymbol{v}_A - \mu \boldsymbol{t}_A \sigma_{NA}) \\ \Delta (\boldsymbol{v}_A g_{NA} - \frac{k}{r}(\boldsymbol{\lambda}_{TA} + \mu \sigma_{NA} \boldsymbol{t}_A)) \end{bmatrix}. \tag{36}$$

The linearization of these quantities can be calculated from the work of Cavalieri and Cardona [10], with the exception of the linearization of the tangential vector $\boldsymbol{t}_A$ that is outlined in Appendix. Here, it is important to remark that since $\boldsymbol{v}_A$ is evaluated at the previous time step, its linearization does not contribute to the Hessian matrix. This assumption leads to a simple formulation with good convergence properties of the nonlinear problem. As it will be shown in the examples, this assumption does not impose a severe restriction on the time-step size necessary to get an accurate solution. Nevertheless, we remark that the linearization of the average normal $\boldsymbol{v}_A$ at the current time step can be incorporated without important modifications to the formulation, with the only inconvenience of a more complex implementation and a larger degree of coupling between degrees of freedom in the problem.

8 Numerical examples

Four numerical examples including finite deformations and large slip are presented to evaluate the robustness and accuracy of the proposed contact algorithm. The examples involve quasi-static simulations and were carried-out in the research finite element code Oofelie [7] where the contact algorithm has been implemented. All pre- and post-processing tasks were performed using the software SAMCEF Field [57].

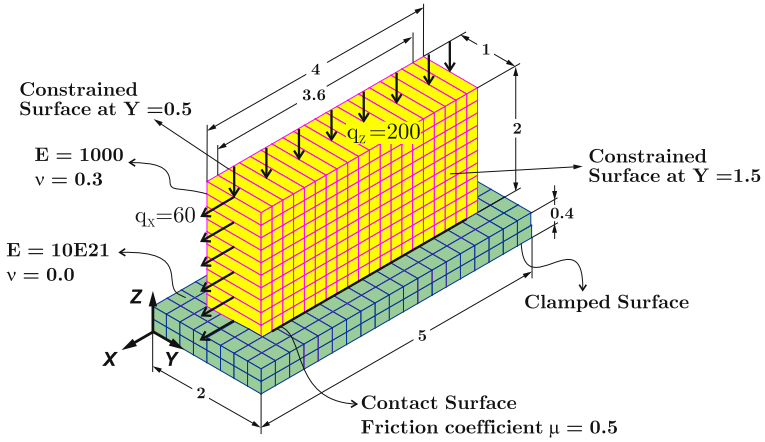

Fig. 4 Elastic body pressured with a rigid surface and pulled tangentially

8.1 Validation example I. Friction test

This test represents an important validation example to study frictional contact algorithms. The example has been first proposed by Oden and Pire [46] as a 2D example, whereas more recent solutions can be found in Armero and Petocz [3], Areias et al. [2], Cavalieri and Cardona [9] using a node-to-segment approach, and in the work of Fischer and Wriggers [18] using a 2D mortar approach. In this work, three-dimensional solutions have been computed introducing boundary conditions that match plane strain conditions to reproduce the same results as in Armero and Petocz [3]. The mesh topology, boundary conditions and mechanical properties used in the simulation are shown in Fig. 4. The penalty and the scaling factors are $p = 10^3$ and $k = 1$, respectively. The material behavior is linear elastic. The upper block has a mesh with 462 nodes and 200 hexahedral elements. The length of the contact zone is 3.6, as shown in Fig. 4. A uniform pressure $q_z = 200$ is applied at the top surface of the upper body, producing a deformation against the rigid foundation. Then, another pressure $q_x = 60$ acts on one side of the body, pulling it in the X-direction. The solution shows agreement with that in [3]. Figure 5(a) shows a numerical comparison of the normal and tangential stresses at the contact interface and Fig. 5(b) shows the residue evolution, giving a quadratic convergence rate.

8.2 Validation example II. Pulling of a plug through a channel

The example presented in this section consists of a block which is pulled through a channel with a corner, see Fig. 6(a). An initial penetration of 1 mm between the slider and the channel is introduced to generate the normal contact pressure. The process is simulated with a uniformly increasing displacement of the slider imposed in 30 equal time steps, going from left to right along a distance of 16 mm. The material behavior of both bodies is that of a compressible Neo-Hookean solid, with the stored energy density expressed as

$$W(I, J) = \frac{\mu}{2}(I - 3 - 2\log J) + \frac{\lambda}{2}(J - 1)^2, \tag{37}$$

where λ and μ are the first and second Lamé parameters, respectively, I is the first invariant of the deviatoric part of the left Cauchy–Green deformation tensor and J is the determinant

Fig. 5 Numerical solutions for the validation example I

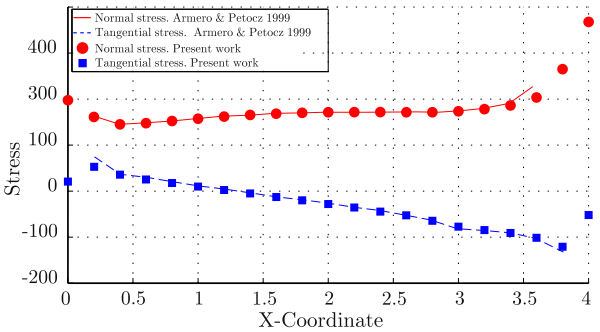

(a) Normal and tangential stress variation at the contact interface. Numerical solutions compared with [3].

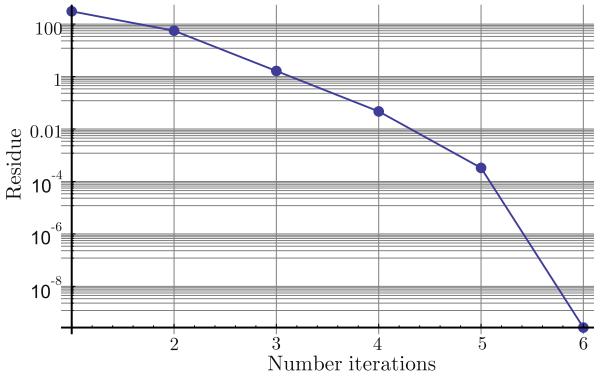

(b) Residue evolution for the friction test.

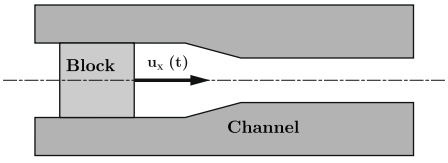

(a) Channel-like die.

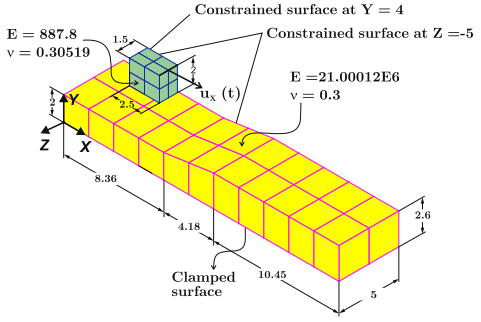

(b) Mesh topology and boundary conditions.

Fig. 6 Problem description of a block through a channel

of the deformation gradient. Figure 6(b) shows the mesh topology and mechanical properties of the example. Friction is modeled by a Coulomb law with a friction coefficient of $\mu = 0.1$. The penalty and scaling factors are both equal to 1×10^4. Due to symmetry, only one quarter of the problem is analyzed. The non-mortar side is selected to be the contact surface of the slider whereas the mortar side is given by the channel contact surface.

It is well known that for this example the convergence rate decreases when using classical node-to-segment approaches and, additionally, solid elements can exhibit an excessive

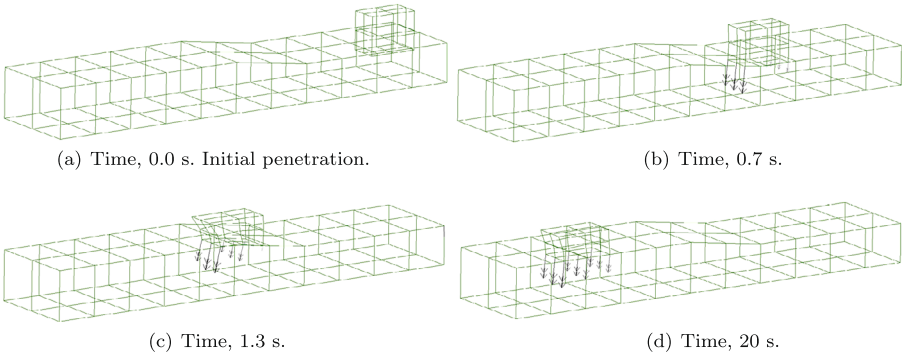

(a) Time, 0.0 s. Initial penetration. (b) Time, 0.7 s.

(c) Time, 1.3 s. (d) Time, 20 s.

Fig. 7 Example with large slip. Deformation and contact pressure vectors at different time steps

Fig. 8 Total tangential reaction. Comparison with solution of Krstulovic-Opara et al. [41]

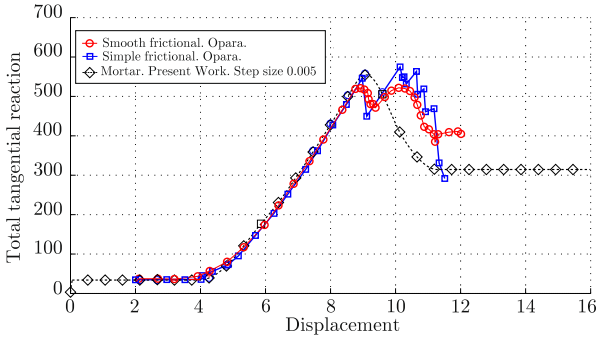

distortion [18]. This effect is due to the fact that reaction forces appear suddenly and are concentrated in small areas, like at the beginning of the channel ramp. To alleviate these drawbacks, the use of smooth contact surfaces, for example, C^1 surfaces, B-splines and others have been proposed; see, for example, the works of Stadler et al. [62] and Krstulovic-Opara et al. [41]. However, it is important to remark that when a node-to-segment contact algorithm is used in combination with high order solid elements, the smoothing techniques of the contact surfaces produce oscillations in the contact pressures. Furthermore, despite smoothing, these algorithms do not pass the contact patch tests [8]. The isogeometric analysis applied to frictional contact problems presented by De Lorenzis et al. [14] could help to overcome this drawback; however, in the mentioned work, the integration is carried out without segmentation of the contact surfaces, which could introduce errors for a general discretization. Errors can be reduced by increasing the number of integration points on the contact surface [17].

As it is shown in this example, the mortar formulation does not present these inconveniences. Figure 7 shows the slider evolution in time where the vectors represent the contact pressures. Note that the slider could pass the channel corner without oscillations of the contact pressure vectors. Horizontal reactions are evaluated at nodes where the displacement is imposed as depicted in Fig. 8. Numerical solutions displayed in Fig. 8 were made using a time step of 0.005. The present mortar approach is in agreement with results of the bibliography; however, as a remarkable difference, smooth solutions of the reaction forces are achieved, while the node-to-segment approach showed strong oscillations in the response.

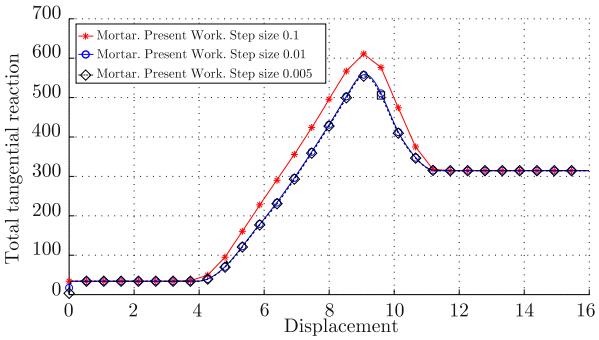

Fig. 9 Total tangential reaction. Comparison of results for different time steps

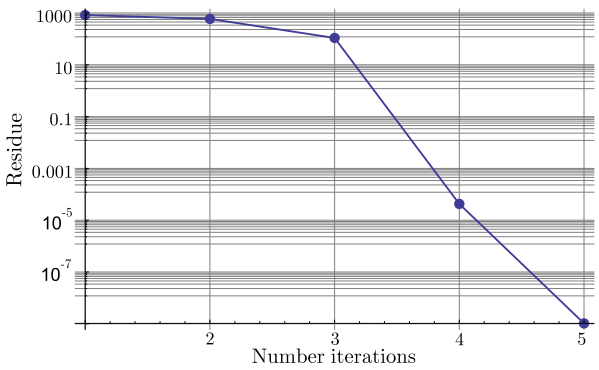

Fig. 10 Residue evolution for a typical time step for the pulling of a plug problem

In order to study the influence of calculating the mean normal vector $\boldsymbol{\nu}_A$ at the previous time step, different computations were performed for various time step values, and the computed tangential and normal reaction forces were compared. The time steps selected for the numerical experiments were: 0.1, 0.01 and 0.005. Solutions using these time steps are plotted in Fig. 9. The differences in the computed normal and tangential reaction forces are negligible, showing that using explicit forms of the mean normal vector does not have a strong influence on the results accuracy.

Figure 10 shows the residue evolution for a typical time step, giving a quadratic convergence rate.

8.3 Validation example III. Two blocks friction test

The test presented in this section is based on a bidimensional example proposed in Hammer's doctoral thesis [26]. A three-dimensional version of this problem has been defined by introducing boundary conditions that match plane strain state. The dimensions and mesh topology are shown in Fig. 11. The mesh has 100 nodes and 39 hexahedral linear finite elements as shown in Fig. 11(a). The material behavior of both bodies is compressible Neo-Hookean with the same stored energy density function as that presented in Eq. (37). Figure 11(a) shows the mechanical properties used in the example. The penalty and the scaling factors are 1×10^{14} and 1×10^{6}, respectively.

At the beginning of the simulation, there is an initial gap of 1 mm between the bodies. This gap is introduced to demonstrate that the implementation is able to capture new contact surfaces, see Fig. 12(a). Then, the upper block is moved downwards in the vertical direction

Fig. 11 Validation example III

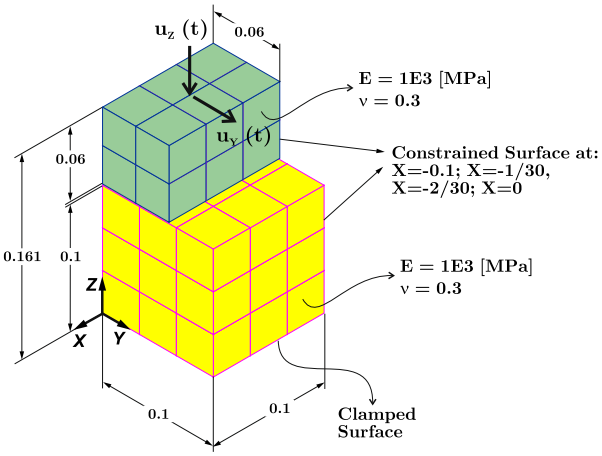

(a) Mechanical properties and boundary conditions.

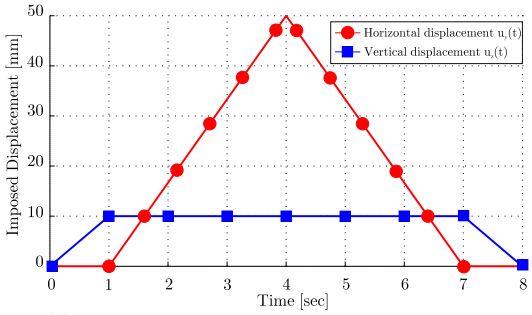

(b) Imposed displacements on the top side of the block.

with a movement law as shown in Fig. 11(b). At the time of 1 s, the vertical displacement $u_z(t)$ is 10 mm. The deformation state at this moment is shown in Fig. 12(b). After 1.6 s, the upper body starts to slip, changing the contact status from stick to slip. Figure 12(c) shows the deformation of both blocks due to the friction forces. Then, the upper block is moved in the Y-direction with a horizontal displacement u_y, until arriving at 50 mm at time 4 s, see Fig. 12(d). After 4 s the movement direction changes and continues until the time of 7 s. Here, the upper block starts lifting to the initial position which is reached at the time of 8 s. The total horizontal and vertical reactions forces evaluated on the top side of the upper block are compared with those computed by Hammer [26]. Both solutions are presented in Fig. 13(a) showing almost perfect agreement. Figure 13(b) displays the residue evolution for a typical time step, showing quadratic convergence.

8.4 Validation example IV. Frictional ironing problem

The fourth example, depicted in Fig. 14, corresponds to the so-called frictional ironing problem. It was originally presented in the work of Puso et al. [54], where they solved this problem by using a mortar based contact formulation with a penalty regularization scheme. Similar examples were proposed by Gitterle [24] who used dual Lagrange multipliers, whereas Temizer [64] and De Lorenzis et al. [14] solved the problem with a kinematic description obtained by using isogeometric analysis.

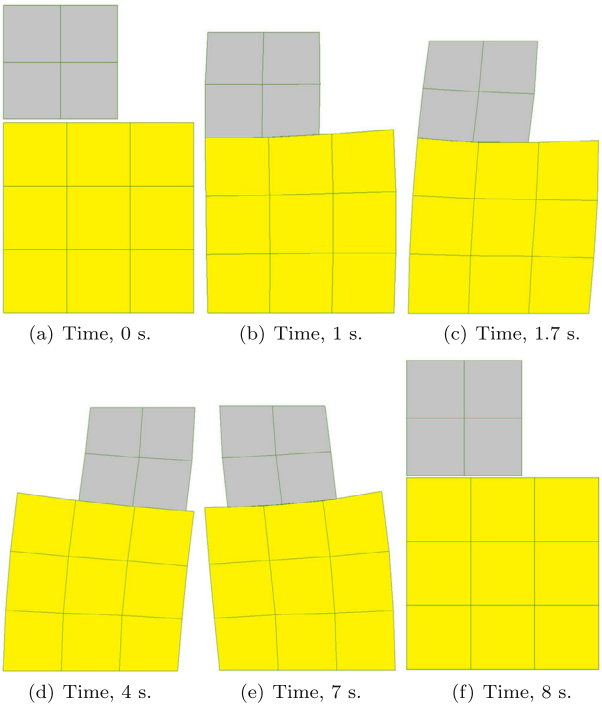

(a) Time, 0 s. (b) Time, 1 s. (c) Time, 1.7 s.

(d) Time, 4 s. (e) Time, 7 s. (f) Time, 8 s.

Fig. 12 Validation example III. Deformation evolution

In this example, a cylindrical die with $E = 1000$ and $\nu = 0.3$ is pressed into an elastic block with $E = 1$ and $\nu = 0.4999$. The material behavior for both bodies is compressible Neo-Hookean with the same stored energy density function as that presented in Eq. (37). The penalty and scaling factors are both equal to 1×10^4. The discretization is performed using eight-nodes hexahedral finite elements. The die is pressed into the block by a prescribed vertical displacement u_Y which varies from 0 to 0.8 m in the negative Y-direction. Then, the vertical displacement u_Y is held constant at 0.8 and at this instant, the die begins to slide with a prescribed horizontal displacement u_X from 0 to 7.13 in 0.45 s. The time step used in the simulation is constant and equal to 0.01. In order to evaluate the robustness of the algorithm, two mesh sizes for the block are proposed. The element size for the coarse mesh is $(X \times Y \times Z)$ $0.45 \times 0.5 \times 0.45$, meanwhile it is $0.225 \times 0.5 \times 0.4$ for the finer mesh.

Figure 14(a) shows the boundary conditions and the mesh topology for the coarse block mesh. Figures 14(b)–(d) show the deformed configurations at different stages. From the pictures, it can be seen that large finite deformations are produced. At the beginning, when the prescribed horizontal displacement u_X starts to act on the die, the contact is mainly in stick. Later on, when the tangential contact forces are equal to the coefficient of friction multiplied by the normal contact forces, the contact state changes to sliding and slip occurs. These stages can be recognized in Fig. 15, where the normal and tangential reaction forces for the two kind of meshes are plotted. As it can be seen, in the coarse mesh case, very small oscillations of the tangential and normal reaction forces are displayed, which are almost completely smoothed out in the fine mesh computation. Figure 16 shows the residue evolution giving a quadratic convergence rate.

Fig. 13 Numerical solutions for the validation example III

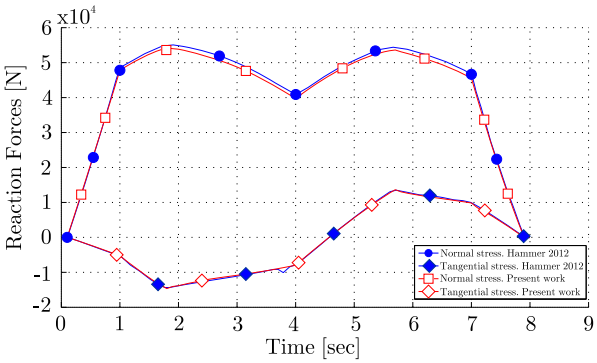

(a) Horizontal and vertical reaction forces evaluated on the top side of the upper block.

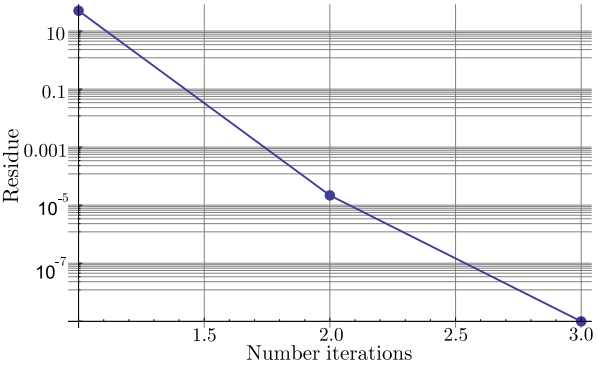

(b) Residue evolution for typical time step in the validation example III.

9 Conclusions

In this work, a new contact algorithm using an augmented Lagrangian method and a mortar approach is presented. The algorithm has three main features: it allows solving the equations with a semismooth Newton method and avoiding the programming complications of algorithms based on activation/deactivation of constraints with a two-leveled iterative loop, it is applicable to problems with non-conforming meshes, and the user does not need to define a penalty parameter. The equations for the computation of the residual forces and tangent matrices were presented. The presented numerical examples demonstrated the ability of the scheme to represent frictional contact problems with small and large displacements. Finally, quadratic convergence rate with a small number of iterations has been achieved in all examples.

Acknowledgements This work has received financial support from Consejo Nacional de Investigaciones Científicas y Técnicas (CONICET), PIP 2011/01105, and from Universidad Nacional del Litoral (CAI+D 2011).

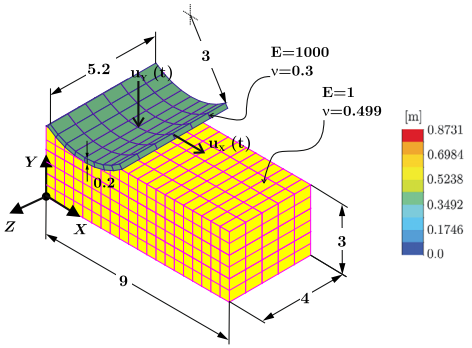

(a) Mesh topology and boundary conditions.

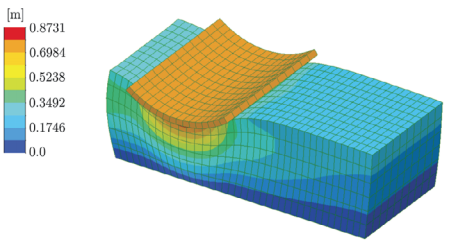

(b) Time, 0.7 s.

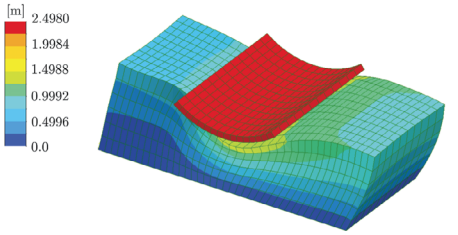

(c) Time, 1.3 s.

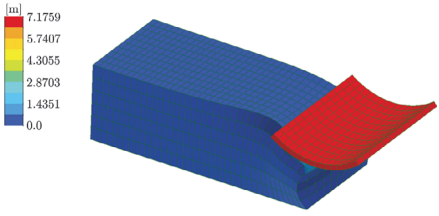

(d) Time, 20 s.

Fig. 14 Ironing example. Mesh topology and deformed configurations for different time steps (Color figure online)

Fig. 15 Normal and tangential reaction forces at the upper surface of the die

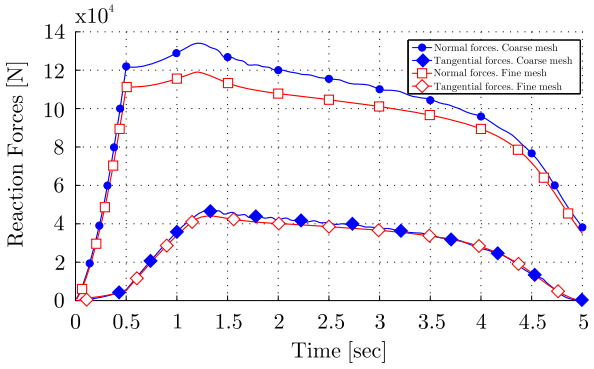

Appendix

The linearization of the tangential vector $\boldsymbol{t}_A$ is presented. The tangential vector $\boldsymbol{t}$ is used in the slip status, thus

$$\boldsymbol{t}_A = \frac{\boldsymbol{\sigma}_{TA}}{\|\boldsymbol{\sigma}_{TA}\|} = \frac{\boldsymbol{\sigma}_{TA}}{-\mu\sigma_{NA}}. \tag{38}$$

The linearization operator Δ applied to Eq. (38) yields

$$\Delta\boldsymbol{t}_A = \frac{[\boldsymbol{I} - \boldsymbol{t}_A \otimes \boldsymbol{t}_A]\Delta\boldsymbol{\sigma}_A}{\|\boldsymbol{\sigma}_{TA}\|} = \frac{[\boldsymbol{I} - \boldsymbol{t}_A \otimes \boldsymbol{t}_A]\Delta\boldsymbol{\sigma}_A}{-\mu\sigma_{NA}}. \tag{39}$$

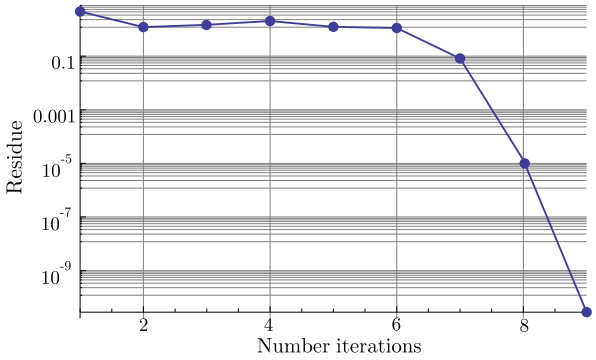

Fig. 16 Residue evolution for a typical time step in the ironing problem

After some algebraic manipulations, the linearization of the tangential vector is written as

$$\Delta \boldsymbol{t}_A = -\frac{\boldsymbol{I} - \boldsymbol{t}_A \otimes \boldsymbol{t}_A - \boldsymbol{v}_A \otimes \boldsymbol{v}_A}{\mu \sigma_{NA}} \Delta \boldsymbol{\sigma}_A + \frac{\boldsymbol{v}_A \otimes \boldsymbol{\sigma}_A + (\boldsymbol{I} - \boldsymbol{t}_A \otimes \boldsymbol{t}_A)\sigma_{NA}}{\mu \sigma_{NA}} \Delta \boldsymbol{v}_A. \tag{40}$$

If the variation of the normal vector $\boldsymbol{v}_A$ is neglected, i.e., if the normal vector is computed at the previous time step, the final expression is given by

$$\Delta \boldsymbol{t}_A = -\frac{\boldsymbol{I} - \boldsymbol{t}_A \otimes \boldsymbol{t}_A - \boldsymbol{v}_A \otimes \boldsymbol{v}_A}{\mu \sigma_{NA}} \Delta \boldsymbol{\sigma}_A. \tag{41}$$

References

1. Alart, P., Curnier, A.: A mixed formulation for frictional contact problems prone to Newton like solution methods. Comput. Methods Appl. Mech. Eng. **92**(3), 353–375 (1991). doi:10.1016/0045-7825(91)90022-X, http://www.sciencedirect.com/science/article/pii/004578259190022X
2. Areias, P.M.A., César de Sá, J.M.A., Conceiçao António, C.A.: Algorithms for the analysis of 3D finite strain contact problems. Int. J. Numer. Methods Eng. **61**, 1107–1151 (2004)
3. Armero, F., Petocz, E.: A new dissipative time-stepping algorithm for frictional contact problems: formulation and analysis. Comput. Methods Appl. Mech. Eng. **179**, 151–178 (1999)
4. Bernardi, C., Maday, Y., Patera, A.: A new nonconforming approach to domain decomposition: the mortar element method. In: Brezia, H., Lions, J. (eds.) Nonlinear Partial Differential Equations and Their Applications, pp. 13–51. Pitman/Wiley, London/New York (1992)
5. Bowling, A., Flickinger, D., Harmeyer, S.: Energetically consistent simulation of simultaneous impacts and contacts in multibody systems with friction. Multibody Syst. Dyn. **22**, 27–45 (2009)
6. Brezzi, F., Fortin, M.: Mixed and Hybrid Finite Element Methods. Springer, New York (1991)
7. Cardona, A., Igor, K., Geradin, M.: Design of a new finite element programming environment. Eng. Comput. **11**, 365–381 (1994)
8. Cavalieri, F.: Multiaxial fatigue and wear design in mechanical components at high temperature. Thesis, Universidad Nacional del Litoral, http://bibliotecavirtual.unl.edu.ar:8180/tesis/handle/1/200 (2010)
9. Cavalieri, F.J., Cardona, A.: An augmented Lagrangian method to solve 3D contact problems. Lat. Am. Appl. Res. **42**(201), 281–289 (2012)
10. Cavalieri, F.J., Cardona, A.: An augmented Lagrangian technique combined with a mortar algorithm for modelling mechanical contact problems. Int. J. Numer. Methods Eng. **93**(4), 420–442 (2013)
11. Cavalieri, F.J., Cardona, A.: Three-dimensional numerical solution for wear prediction using a mortar contact algorithm. Int. J. Numer. Methods Eng. **96**(8), 467–486 (2013)
12. Cavalieri, F.J., Fachinotti, V., Cardona, A.: A mortar contact algorithm for three-dimensional elasticity problems. Rev. Int. Métod. Numér. Cálc. Diseño Ing. **28**(2), 80–92 (2012)
13. Cichosz, T., Bischoff, M.: Consistent treatment of boundaries with mortar contact formulations using dual Lagrange multipliers. Comput. Methods Appl. Mech. Eng. **200**(9–12), 1317–1332 (2011)

14. De Lorenzis, L., Temizer, A., Wriggers, P., Zavarise, G.: A large deformation frictional contact formulation using NURBS-based isogeometric analysis. Int. J. Numer. Methods Eng. **87**(13), 1278–1300 (2011)
15. De Lorenzis, L., Wriggers, P., Zavarise, G.: A mortar formulation for 3D large deformation contact using NURBS-based isogeometric analysis and the augmented Lagrangian method. Comput. Mech. **49**(1), 1–20 (2012)
16. Esche, S., Kinzel, G., Altan, T.: Issues in convergence improvement for non-linear finite element programs. Int. J. Numer. Methods Eng. **40**, 4577–4594 (1997)
17. Fischer, K., Wriggers, P.: Frictionless 2D contact formulations for finite deformations based on the mortar method. Comput. Mech. **36**(3), 226–244 (2005)
18. Fischer, K., Wriggers, P.: Mortar based frictional contact formulation for higher order interpolations using the moving friction cone. Comput. Methods Appl. Mech. Eng. **195**(37–40), 5020–5036 (2006)
19. Flores, F.: Un algoritmo de contacto para el análisis explícito de procesos de embutición. Métod. Numér. Cálc. Diseño Ing. **16**, 421–432 (2000)
20. Flores, P., Ambrósio, J.: On the contact detection for contact-impact analysis in multibody systems. Multibody Syst. Dyn. **24**, 103–122 (2010)
21. Förg, M., Pfeiffer, F., Ulbrich, H.: Simulation of unilateral constrained systems with many bodies. Multibody Syst. Dyn. **14**, 137–154 (2005)
22. Gamez-Montero, P., Zárate, F., Sánchez, M., Castilla, R., Codina, E.: El problema del contacto en bombas de engranajes de perfil troncoidal. Métod. Numér. Cálc. Diseño Ing. **21**, 213–229 (2005)
23. Giannakopoulos, A.: The radial mapping method for the integration of friction constitutive relations. Comput. Struct. **6**, 281–290 (1989)
24. Gitterle, M.: A dual mortar formulation for finite deformation frictional contact problems including wear and thermal coupling. Ph.D. thesis, Fakultät für Maschinenwesen der Technischen Universität München (2012)
25. Gitterle, M., Popp, A., Gee, M.W., Wall, W.A.: Finite deformation frictional mortar contact using a semi-smooth Newton method with consistent linearization. Int. J. Numer. Methods Eng. **84**(5), 543–571 (2010). doi:10.1002/nme.2907
26. Hammer, M.: Frictional mortar contact for finite deformation problems with synthetic contact kinematics. Ph.D. thesis, Institut für Festigkeitslehre der Technischen Universität Graz (2012)
27. Hartmann, S., Oliver, J., Weyler, R., Cante, J., Hernández, J.: A contact domain method for large deformation frictional contact problems. Part 2: numerical aspects. Comput. Methods Appl. Mech. Eng. **198**(33–36), 2607–2631 (2009). doi:10.1016/j.cma.2009.03.009, http://www.sciencedirect.com/science/article/pii/S0045782509001297
28. Hartmann, S., Ramm, E.: A mortar based contact formulation for non-linear dynamics using dual Lagrange multipliers. Finite Elem. Anal. Des. **44**(5), 245–258 (2008)
29. Hüeber, S., Wohlmuth, B.: A primal dual active set strategy for non-linear multibody contact problems. Comput. Methods Appl. Mech. Eng. **194**(27–29), 3147–3166 (2005)
30. Hüeber, S., Wohlmuth, B.: Thermo-mechanical contact problems on non-matching meshes. Comput. Methods Appl. Mech. Eng. **198**(15–16), 1338–1350 (2009)
31. Heegaard, J., Curnier, A.: An augmented Lagrangian method for discrete large slip contact problems. Int. J. Numer. Methods Eng. **36**(4), 569–593 (1993)
32. Heintz, P., Hansbo, P.: Stabilized Lagrange multiplier methods for bilateral elastic contact with friction. Comput. Methods Appl. Mech. Eng. **195**(33–36), 4323–4333 (2006)
33. Hesch, C., Betsch, P.: Transient three-dimensional domain decomposition problems: frame-indifferent mortar constraints and conserving integration. Int. J. Numer. Methods Eng. **82**(3), 329–358 (2010)
34. Hesch, C., Betsch, P.: Transient three-dimensional contact problems: mortar method. Mixed methods and conserving integration. Comput. Mech. **48**(4), 461–475 (2011)
35. Hüeber, S., Mair, M., Wohlmuth, B.I.: A priori error estimates and an inexact primal-dual active set strategy for linear and quadratic finite elements applied to multibody contact problems. Appl. Numer. Math. **54**(3–4), 555–576 (2005)
36. Ignesti, M., Innocenti, A., Marini, L., Meli, E., Rindi, A.: Development of a model for the simultaneous analysis of wheel and rail wear in railway systems. Multibody Syst. Dyn. **31**(2), 191–240 (2014)
37. Johnson, K.: Contact Mechanics. Cambridge University Press, Cambridge (1987)
38. Jones, R., Papadopoulos, P.: A novel three-dimensional contact finite element based on smooth pressure interpolations. Int. J. Numer. Methods Eng. **51**(7), 791–811 (2001)
39. Kikuchi, N., Oden, J.: Contact Problems in Elasticity: a Study of Variational Inequalities and Finite Element Methods. SIAM, Philadelphia (1988)
40. Kim, J., Youn, S.: Isogeometric contact analysis using mortar method. Int. J. Numer. Methods Eng. **89**(12), 1559–1581 (2012)

41. Krstulovic-Opara, L., Wriggers, P., Korelc, J.: Symbolically generated 3D smooth polynomial frictional contact element based on the quartic Bézier surfaces. In: Oñate, E., Bugeda, G., Suárez, B. (eds.) CD-ROM Proceedings of the European Congress on Computational Methods in Applied Sciences and Engineering. ECCOMAS, Barcelona (2000)
42. Laursen, T.: Formulation and treatment of frictional contact problems using finite elements. Ph.D. Thesis, Stanford University, USA (1992)
43. Laursen, T.: Computational Contact and Impact Mechanics. Springer, Berlin (2002)
44. McDevitt, T.W., Laursen, T.A.: A mortar-finite element formulation for frictional contact problems. Int. J. Numer. Methods Eng. **48**(10), 1525–1547 (2000)
45. Moreau, J.: Application of convex analysis to some problems of dry friction. In: Zorski, H. (ed.) Trends of Pure Mathematics Applied to Mechanics, vol. 11. Pitma, London (1979)
46. Oden, J., Pire, E.: Algorithms and numerical results for finite element approximation of contact problems with non-classical friction laws. Comput. Struct. **19**(1–2), 137–147 (1984)
47. Oliver, J., Hartmann, S., Cante, J., Weyler, R., Hernández, J.: A contact domain method for large deformation frictional contact problems. Part 1: theoretical basis. Comput. Methods Appl. Mech. Eng. **198**(33–36), 2591–2606 (2009). doi:10.1016/j.cma.2009.03.006, http://www.sciencedirect.com/science/article/pii/S004578250900125X
48. Papadopoulos, P., Solberg, J.: A Lagrange multiplier method for the finite element solution of frictionless contact problems. Math. Comput. Model. **28**(4–8), 373–384 (1998)
49. Papadopoulos, P., Taylor, R.: A mixed formulation for the finite element solution of contact problems. Technical Report UCB/ SEMM Report 90/18, University of California at Berkeley (1990)
50. Popp, A., Gee, M.W., Wall, W.A.: A finite deformation mortar contact formulation using a primal dual active set strategy. Int. J. Numer. Methods Eng. **79**(11), 1354–1391 (2009). doi:10.1002/nme.2614
51. Popp, A., Gitterle, M., Gee, M.W., Wall, W.: A dual mortar approach for 3D finite deformation contact with consistent linearization. Int. J. Numer. Methods Eng. **83**(11), 1428–1465 (2010)
52. Popp, A., Seitz, A., Gee, M.W., Wall, W.A.: Improved robustness and consistency of 3D contact algorithms based on a dual mortar approach. Comput. Methods Appl. Mech. Eng. **264**, 67–80 (2013)
53. Puso, M.: A 3D mortar method for solid mechanics. Int. J. Numer. Methods Eng. **59**(3), 315–336 (2004)
54. Puso, M., Laursen, T.: A mortar-finite element formulation for frictional contact problems. Comput. Methods Appl. Math. **193**, 60l–629 (2004)
55. Puso, M., Laursen, T.: A mortar segment-to-segment frictional contact method for large deformations. Comput. Methods Appl. Mech. Eng. **193**(45–47), 4891–4913 (2004)
56. Puso, M.A., Laursen, T.A.: A mortar segment-to-segment contact method for large deformation solid mechanics. Comput. Methods Appl. Mech. Eng. **193**(6–8), 601–629 (2004). doi:10.1016/j.cma.2003.10.010, http://www.sciencedirect.com/science/article/pii/S0045782503005802
57. SAMCEF: Mecano V13 user manual. LMS-Samtech S.A. (2007). http://www.lmsintl.com
58. Simo, J., Laursen, T.: An augmented Lagrangian treatment of contact problems involving friction. Comput. Struct. **42**, 97–116 (1992)
59. Simo, J.C., Hughes, T.J.R.: Computational Inelasticity. Springer, Berlin (1998)
60. Solberg, J., Jones, R., Papadopoulos, P.: A family of simple two-pass dual formulations for the finite element solution of contact problems. Comput. Methods Appl. Mech. Eng. **196**(4–6), 782–802 (2007)
61. Solberg, J., Papadopoulos, P.: An analysis of dual formulations for the finite element solution of two-body contact problems. Comput. Methods Appl. Mech. Eng. **194**(25–26), 2734–2780 (2005)
62. Stadler, M., Holzapfel, G.A.: Subdivision schemes for smooth contact surfaces of arbitrary mesh topology in 3D. Int. J. Numer. Methods Eng. **60**(7), 1161–1195 (2004). doi:10.1002/nme.1001
63. Temizer, A.: A mixed formulation of mortar-based frictionless contact. Comput. Methods Appl. Mech. Eng. **223–224**, 173–185 (2012)
64. Temizer, A.: A mixed formulation of mortar-based contact with friction. Comput. Methods Appl. Mech. Eng. **255**, 183–195 (2013)
65. Temizer, A., Wriggers, P., Hughes, J.: Three-dimensional mortar-based frictional contact treatment in isogeometric analysis with NURBS. Comput. Methods Appl. Mech. Eng. **209–212**, 115–128 (2012)
66. Tur, M., Fuenmayor, F., Wriggers, P.: A mortar-based frictional contact formulation for large deformations using Lagrange multipliers. Comput. Methods Appl. Mech. Eng. **198**(37–40), 2860–2873 (2009). doi:10.1016/j.cma.2009.04.007, http://www.sciencedirect.com/science/article/pii/S0045782509001595
67. Wohlmuth, B.: A mortar finite element method using dual spaces for the Lagrange multiplier. SIAM J. Numer. Anal. **38**(3), 989–1012 (2000)
68. Wriggers, P.: Computational Contact Mechanics. Wiley and Sons, New York (2002)
69. Yang, B., Laursen, T., Meng, X.: Two dimensional mortar contact methods for large deformation frictional sliding. Int. J. Numer. Methods Eng. **62**(9), 1183–1225 (2005)